Section 9

Development of and studies with coupled and Earth system models and data assimilation systems.

Numerical simulations of Typhoon Chanthu (2021) by two nonhydrostatic atmosphere models and an atmosphere-wave ocean coupled model

Akiyoshi Wada, Wataru Yanase, and Satoki Tsujino

Meteorological Research Institute, Tsukuba, Ibaraki, 305-0052, JAPAN

[1]awada@mri-jma.go.jp

1. Introduction

A tropical depression developed to a tropical storm (named Chanthu) around ($14.6\,^{\circ}$N, $138.0\,^{\circ}$E) at 12 UTC on 6 September 2021. Chanthu moved northwestward and then westward in its intensification phase. Chanthu reached the minimum central pressure of 905 hPa at 18 UTC on 10 September over the sea north of Luzon Island. Then, Chanthu changed the moving direction to the north and passed east of Taiwan while the tropical cyclone (TC) was weakening. The TC entered the East China Sea on 13 September and stagnated from 15 to 16 September. After the stagnation, the TC moved northeastward and made landfall in Japan around 18 UTC on 17 September.

There are two issues on the track forecast of Chanthu and the other two in the intensity forecast. First, the Japan Meteorological Agency (JMA) forecasted that Chanthu moved more northward than the observed track in the intensification phase. Second, the forecast error of the TC track increased on around 15 September in the East China Sea. Third, the JMA forecast tended to overly develop the TC during the mature and decaying phases. Last, the TC redeveloped in the East China Sea contrary to the forecast. This report addresses the second and third subjects. Numerical simulations were conducted for Chanthu by using an operational nonhydrostatic atmosphere model (asuca: Asuca is a System based on a Unified Concept for Atmosphere), a nonhydrostatic atmosphere model (NHM, Wada et al., 2018) and the coupled atmosphere-wave-ocean model (CPL, Wada et al., 2018).

2. Experimental design

Table 1 shows a list of numerical simulations. Each initial time was 0000 UTC on 9 September 2021. The computational domain was 1500 x 2700 km with a grid spacing of 1.5 km (Fig. 1a). The number of the vertical layer was 55 for NHM and CPL and 96 for asuca. The top height was approximately 27 km for the NHM and CPL and approximately 37 km for the asuca. The integration time of all simulations was 144 hours.

Table1 List of numerical simulations

Name	Model	IRE	Cumulus Parameterization
NHM	NHM	0.2	None
CPL	CPL	0.2	None
asuca(1.0)	asuca	1.0	KF: Kain and Fritsch (1990)
asuca(0.15)	asuca	0.15	KF: Kain and Fritsch (1990)
asuca(0.05)	asuca	0.05	KF: Kain and Fritsch (1990)

The time step was 3 seconds in the NHM, the asuca, and the atmospheric part of CPL, 18 seconds for the ocean model incorporated into the CPL, and 6 minutes for the ocean surface wave model incorporated into the CPL. The cumulus parameterization of Kain and Fritsch (1990) (KF in Table 1) was used only for the asuca. The setting of KF was the same as that in the local forecast model operationally used in JMA. The atmospheric boundary-layer scheme used in the NHM and CPL was the same as that in Wada et al. (2018), while Mellor-Yamada-Nakanishi-Niino level 2.5 closure scheme (e.g., Nakanishi and Niino, 2009) was used in the numerical simulations conducted by the asuca. The inhibition rate of evaporation (IRE) of rain, snow, and graupel included in the cloud physics for the NHM and CPL was 0.2, while three sensitivity experiments were conducted by the asuca on the IRE by using the following three values (1.0, 0.15, 0.05).

The JMA global objective analysis with the horizontal resolution of 20 km and the JMA North Pacific Ocean analysis with the horizontal resolution of 0.5° were used for creating atmospheric and oceanic initial conditions and atmospheric lateral boundary conditions every 6 hours. As for the initial condition of sea surface temperature (SST), the Optimally Interpolated SST (OISST) daily product with the horizontal resolution of 0.25°, obtained from the Remote Sensing Systems (http://www.remss.com) was used.

The Regional Specialized Meteorological Center (RSMC) Tokyo best track data (https://www.jma.go.jp/jma/jma-eng/jma-center/rsmc-hp-pub-eg/besttrack.html) was used to validate the results of numerical simulations.
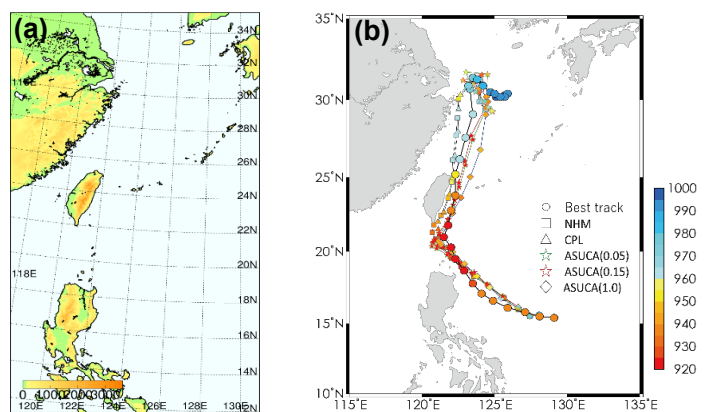

Figure 1 (a) Computational domain. (b) Track simulation results with the RSMC best track. Colors in the marks indicate the value of central pressure (hPa).

3. Results

3.1 Tracks

Figure 1b shows the results of simulated tracks and central pressures in all simulations together with the RSMC Tokyo best track data. All simulated tracks clearly show a northward deflection in the intensification phase compared to the best track when the TC actually moved westward. In the weakening phase of Chanthu, the variation in the simulated tracks among the simulations by the asuca with different IRE was greater than that in the intensification phase. The increase in IRE (from 0.05 to 1) in the simulations by the asuca led to the eastward shift of the simulated track. Compared to the impact of IRE on the tracks simulated by the asuca, there was less impact of ocean coupling on the tracks simulated by the NHM and CPL.

It should be noted that the value of 1.0 on IRE is scientifically valid. In other words, the discrepancy between the simulations and the best track suggests that the physical processes in the atmosphere models are not well-tuned.

3.2 Intensity changes

Figure 2 shows the time series of simulated central pressure with the best-track central pressure from 00 UTC on 9 September to 00 UTC on 15 September. The best-track central pressure at 00 UTC on 9 September was actually 935 hPa, which was much lower than the central pressure at the initial time obtained from objectively analysis with the horizontal resolution (20 km) much coarser than 1.5 km. The central pressure in the experiments asuca (0.05) and asuca (0.15) decreased more rapidly than that in the experiment asuca (1.0) at the early integration time. The rapid lowering was also simulated in the NHM and CPL experiments. The simulated central pressure simulated by the asuca decreased more rapidly for a lower IRE. However, the simulations by the NHM and CPL showed a relatively high value of the minimum central pressures although IRE was close to asuca (0.15). The impact of ocean coupling on simulated central pressures became distinct around 10 September.
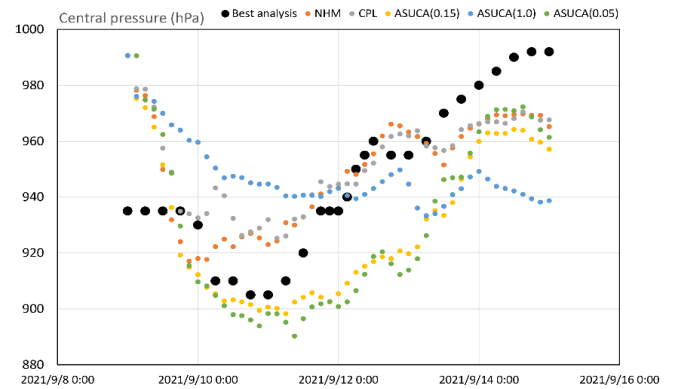

Figure 2 Time series of simulated central pressures with the best-track central pressure (hPa).

3.3 Wind structure in the inner core

Figure 3 shows the horizontal distributions of simulated winds at the height of 20 m. The wind distributions simulated by the NHM and CPL show the asymmetric distribution. The wind distribution simulated in the experiment asuca (1.0) also shows the asymmetric feature, while the axisymmetric feature was found in the wind distribution in the experiments asuca (0.05) and asuca (0.15). The difference in the surface wind distribution corresponded to the simulated intensity (Fig. 2) in that the simulated central pressure was relatively high when the surface wind distribution showed the asymmetric feature.

4. Concluding remarks

The sensitivity to simulated TC to IRE may vary between the NHM and the asuca. In that sense, sensitivity to ocean coupling may also differ between the two models. The results of simulations by the asuca with different IRE suggest that the amount of evaporation cooling due to precipitation does affect the structure and track of simulated Chanthu. How this sensitivity will be changed by the asuca coupled with an ocean model will be a subject in the future.

If a TC in the mature phase is used as a case study, the initial condition should be realistically reproduced to avoid unrealistic decreases in central pressures.
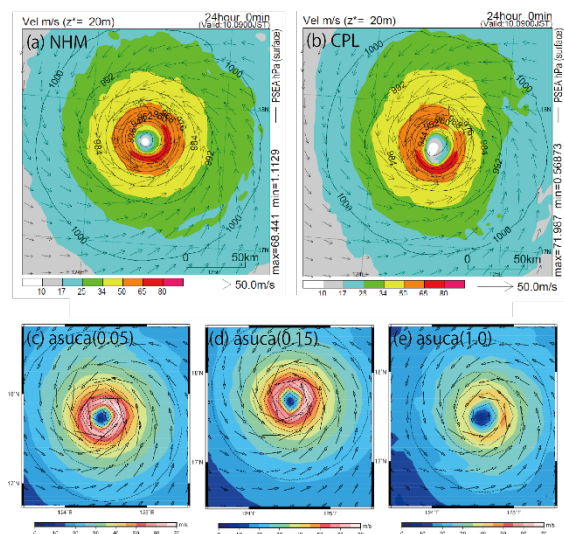

Figure 3 Horizontal distributions of winds at the height of 20 m at 00 UTC on 10 September 2021 simulated by the (a) NHM, (b) CPL and (c-e) asuca (see Table 1 for the difference in the inhibition rates of evaporation of rain, snow, and graupel).

References

Kain, J. S., and J. M. Fritsch (1990). A one-dimensional entraining/detraining plume model and its application in convective parameterization. Journal of the Atmospheric Sciences, 47, 2784-2802.

Nakanishi, M., and H. Niino (2009). Development of an improved turbulence closure model for the atmospheric boundary layer. Journal of the Meteorological Society of Japan, 87, 895-912.

Wada, A., S. Kanada, and H. Yamada (2018). Effect of air–sea environmental conditions and interfacial processes on extremely intense typhoon Haiyan (2013). Journal of Geophysical Research: Atmospheres, 123, 10379-10405.

Numerical simulations of Typhoon Rai (2021) by two nonhydrostatic atmosphere models and an atmosphere-wave ocean coupled model

Akiyoshi Wada, Wataru Yanase, and Satoki Tsujino

Meteorological Research Institute, Tsukuba, Ibaraki, 305-0052, JAPAN

[1]awada@mri-jma.go.jp

1. Introduction

A tropical depression developed to a tropical storm (named Rai) around (6.0°N, 141.0°E) at 06 UTC on 13 December 2021. Rai moved west-northwestward in the intensification phase and then made landfall in the Philippines. Rai reached the minimum central pressure of 915 hPa at 06 UTC on 16 December over the Philippines Sea and at 18 UTC on 18 December after the TC moved into the South China Sea. The double peaks with a central pressure of 915 hPa have never been observed in TCs in December before.

To investigate the possibility of the prediction of the record-breaking double peaks, numerical simulations were conducted for Rai by using an operational nonhydrostatic atmosphere model (asuca: Asuca is a System based on a Unified Concept for Atmosphere), a nonhydrostatic atmosphere model (NHM, Wada et al., 2018) and the coupled atmosphere-wave-ocean model (CPL, Wada et al., 2018).

2. Experimental design

Table 1 shows a list of numerical simulations. Each initial time was 0000 UTC on 13 December 2021. The computational domain was 5000 x 2000 km with a grid spacing of 2 km (Fig. 1a). The number of the vertical layer was 55 for NHM and CPL and 96 for the asuca. The top height was approximately 27 km for NHM and CPL and approximately 37 km for asuca. The integration time in all simulations was 156 hours.

Table1 List of numerical simulations

Name	Model	IRE	Cumulus Parameterization
NHM	NHM	0.2	None
CPL	CPL	0.2	None
asuca (1.0)	asuca	1.0	KF: Kain and Fritsch (1990)
asuca (0.0)	asuca	0.0	KF: Kain and Fritsch (1990)

The time step was 5 seconds for the NHM, the asuca, and the atmospheric part of CPL, 30 seconds for the ocean model incorporated into the CPL, and 6 minutes for the ocean surface wave model incorporated into the CPL. The cumulus parameterization of Kain and Fritsch (1990) (KF in Table 1) was used only for the asuca. The setting of KF was the same as that in the local forecast model operationally used in JMA. The atmospheric boundary-layer scheme used in the NHM and CPL was the same as that in Wada et al. (2018), while Mellor-Yamada-Nakanishi-Niino level 2.5 closure scheme (e.g. Nakanishi and Niino, 2009) was used in the numerical simulations conducted by the asuca. The inhibition rate of evaporation (IRE) of rain, snow, and graupel included in the cloud physics for the NHM and CPL was 0.2, while three sensitivity experiments were conducted by the asuca on the IRE by using the following two values (1.0, 0.0).

The JMA global objective analysis with the horizontal resolution of 20 km and the JMA North Pacific Ocean analysis with the horizontal resolution of 0.5° were used for creating atmospheric and oceanic initial conditions and atmospheric lateral boundary conditions. As for the initial condition of sea surface temperature (SST), the Optimally Interpolated SST (OISST) daily product with the horizontal resolution of 0.25°, obtained from the Remote Sensing Systems (http://www.remss.com) was used. The Regional Specialized Meteorological Center (RSMC) Tokyo best track data (https://www.jma.go.jp/jma/jma-eng/jma-center/rsmc-hp-pub-eg/besttrack.html) was used to validate the results of numerical simulations.
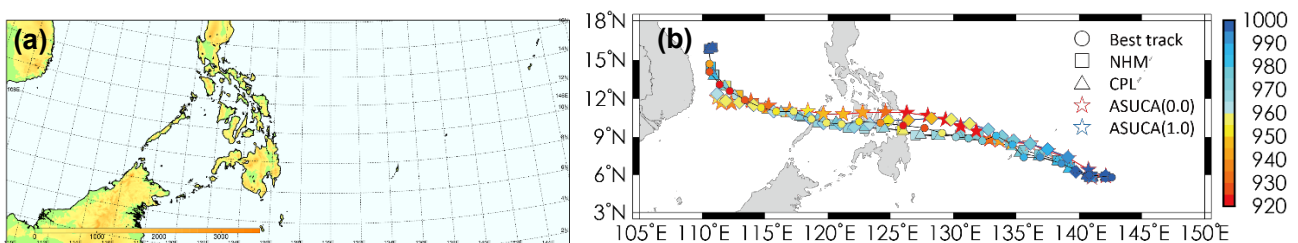

Figure 1 (a) Computational domain. (b) Track simulation results with the RSMC best track. Colors in the marks and vertical bar indicate the value of central pressure (hPa).

3. Results

3.1 Tracks

Figure 1b shows that the tracks in all simulations are in good agreement with the RSMC Tokyo best track data. The tracks simulated by the asuca show a northward deflection compared to the best track before and during making landfall in the Philippines. After the landfall, all simulated tracks show that the moving direction was westward to west-northwestward and then changed to the northward direction at around (12°N, 112.0°E). Around the recurvature

area in the South China Sea, the track of simulated Rai shows a slightly southwestward deflection compared to the best track.

3.2 Intensity changes

Figure 2 shows the time series of simulated central pressure with the best-track central pressure from 00 UTC on 13 December to 12 UTC on 19 December. The simulated central pressure in the experiment asuca (0.0) decreased more rapidly than that in the experiment asuca (1.0). Compared to the results simulated by the asuca, the results simulated by the NHM and CPL show a relatively high value of the minimum central pressures, but the timing of the first peak of simulated minimum central pressure is consistent with that in the best track data.

Around the recurvature area in the South China Sea, the timeseries of minimum central pressure in the RSMC best track data indicates the occurrence of the second peak intensity. The simulated central pressures in the South China Sea was relatively high at the timing compared to the RSMC best track intensity.

Figure 2 Time series of simulated central pressures with the best-track central pressure (hPa).

The impact of ocean coupling on simulated central pressures represented by the difference between the NHM and CPL was distinct at the second peak. Without the ocean coupling, the central pressure simulated by the NHM was the lowest in the South China Sea, while the other simulation showed that the simulated central pressure was the lowest east of the Philippines.

3.3 Rainfall structure

Figure 3 shows the horizontal distributions of simulated hourly rainfall and 89GHz Polarized Corrected Temperature (PCT). The size of the storm's eye simulated by the NHM and CPL was relatively large compared with the eye observed in Fig. 3e. The horizontal distributions of hourly rainfall simulated by the NHM (Fig. 3a) and CPL (Fig. 3b) show an axisymmetric pattern. The east-west spreading simulated rainband on the north side corresponded to that in the satellite analysis (Fig .3e) although the distribution simulated by the NHM differed from that simulated by the CPL. The horizontal distribution in the experiment asuca (0.0) (Fig. 3c) shows an asymmetric pattern with smaller eye than in the NHM and CPL simulations (Figs. 3a, b). However, the size of the storm's eye became large when the IRE was 1.0 (Fig. 3d) since the simulated central pressure in the experiment asuca (1.0) was much higher than that in the experiment asuca (0.0) (Fig. 2).
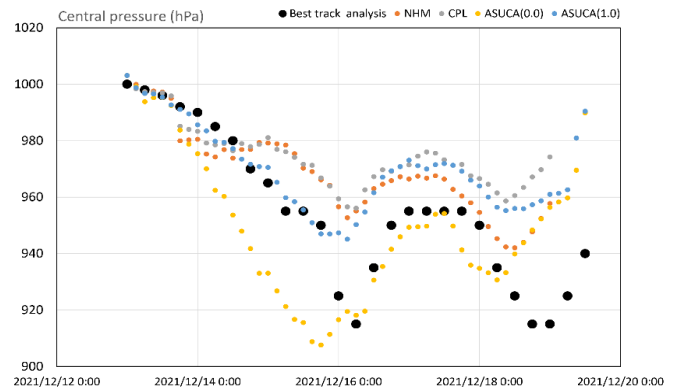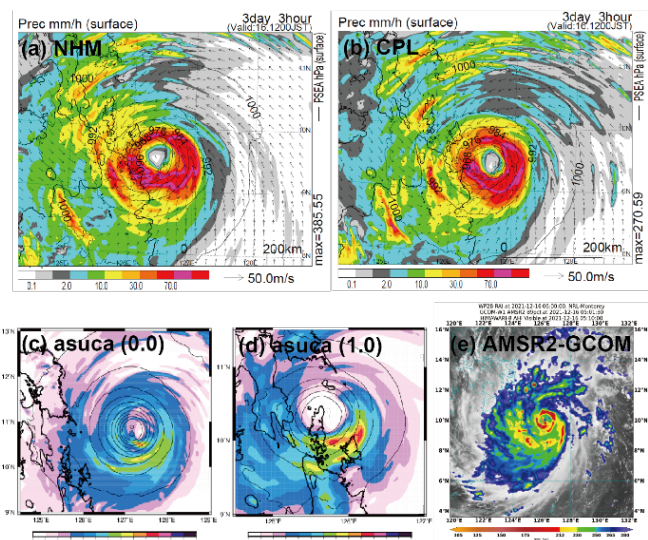

Figure 3 Horizontal distributions of hourly rainfall at 03 UTC on 16 December in 2021 simulated by the (a) NHM, (b) CPL, and (c-d) asuca (see Table 1 for the difference in the IRE). (e) 89GHz PCT at around 05 UTC on 16 December.

4. Concluding remarks

The simulation results successfully reproduced the storm's track and double intensity peaks. However, all models could not quantitatively predict the intensity particularly the peak intensity in the South China Sea. Although the first intensity peak of Rai east of the Philippines was simulated better than the second intensity peak in the South China Sea in the experiment asuca (0.0), the inner-core structure such as the small eye size of the storm and fine eyewall structure before making landfall in the Philippines could not be simulated realistically. The lack of fine inner-core structure of simulated Rai may be the reason why the rapid intensification could not be predicted at all in the first intensity peak and subsequently in the second intensity peak.

References

Kain, J. S., and J. M. Fritsch (1990). A one-dimensional entraining/detraining plume model and its application in convective parameterization. Journal of the Atmospheric Sciences, 47, 2784-2802.

Nakanishi, M., and H. Niino (2009). Development of an improved turbulence closure model for the atmospheric boundary layer. Journal of the Meteorological Society of Japan, 87, 895-912.

Wada, A., S. Kanada, and H. Yamada (2018). Effect of air–sea environmental conditions and interfacial processes on extremely intense typhoon Haiyan (2013). Journal of Geophysical Research: Atmospheres, 123, 10379-10405.

The effects of oceanic initial conditions created from different reanalysis datasets on the intensity prediction of Typhoon Trami (2018)

Akiyoshi Wada

Meteorological Research Institute, Tsukuba, Ibaraki, 305-0052, JAPAN

*awada@mri-jma.go.jp

1. Introduction

Wada (2019) showed the results of numerical simulations on Typhoon Trami (2018) to investigate roles of a mesoscale cold eddy centered at around (21˚N, 129 ˚E) in the rapidly weakening of the intensity from 915 hPa at 06 UTC on 25 September to 950 hPa at 00 UTC on 26 September according to the Regional Specialized Meteorological Center (RSMC) Tokyo best track analysis (https://www.jma.go.jp/jma/jma-eng/jma-center/rsmc-hp-pub-eg/besttrack.html). From the results of ensemble simulations on different oceanic initial conditions, the setting of an unrealistic artificial mesoscale cold eddy was needed to simulate the rapid weakening even when a coupled atmosphere-wave-ocean coupled model was used (Wada, 2021). In the supplement of Wada (2021), the timeseries of tropical cyclone heat potential (TCHP) averaged in a 2˚×2˚ squared area centered at (21˚N, 129˚E) from 19 September to 5 October 2018 showed that the value of TCHP varied depending on the analysis/reanalysis data set although all data sets showed that the TCHP did decrease from 25 September. To understand the difference of the oceanic initial condition attributed to the difference in the oceanic analysis/reanalysis data set on the simulation of Trami, numerical simulations were conducted by using a nonhydrostatic atmosphere model (NHM) and the coupled atmosphere-wave-ocean model (CPL).

2. Experimental design

The list of numerical simulations is shown in Table 1. The initial time of all experiment was 0000 UTC on 23 September in 2018. The computational domain was 2280 x 3120 km with a grid spacing of 2 km (Fig. 1a). The number of the vertical layer was 55 for the NHM and CPL. The top height was approximately 27 km for both NHM and CPL. The integration time in all simulations was 180 hours.

The oceanic reanalysis datasets used in this study were the Four-dimensional variational Ocean ReAnalysis (FORA) dataset (Usui et al. 2017) with a 0.5° horizontal resolution, new data set with a 0.1° horizontal resolution for operational use in Japan Meteorological Agency (JPN), and the Copernicus Marine Environment Monitoring Service GLOBAL_ANALYSISFORECAST _PHY_CPL_001_015 dataset (Lea et al. 2015) with a 0.25° horizontal resolution (ORA5).

It should be noted that an artificial cold eddy (Wada, 2021) was not embedded in the oceanic initial condition in all experiments shown in Table 1. This implies that simulated Trami would overly develop after the rapidly weakening from 25 to 26 September in the NP05_CPL experiment like the result in Wada (2021).

3. Results

Figure 1b shows the results of simulated central pressure positions along with the RSMC best track positions. The effect of the difference in oceanic initial conditions on the track simulation was not significant. This result was also found in the comparison of the simulation results between NHM and CPL. All simulation results clearly show the irregularity of the storm track from 25 to 27 September where Trami-induced sea surface cooling occurred (Wada, 2021). Except the northeastward shift of the simulated track on 27 September, the simulated tracks in all experiments were reasonable to the RSMC best track.

Table1 List of numerical simulations

Name	Model	Oneanic initial data
NP05_NHM	NHM	FORA
NP05_CPL	Coupled NHM-wave-ocean	FORA
NP01_NHM	NHM	JPN
NP01_CPL	Coupled NHM-wave-ocean	JPN
ORA5_NHM	NHM	ORA5
ORA5_CPL	Coupled NHM-wave-ocean	ORA5

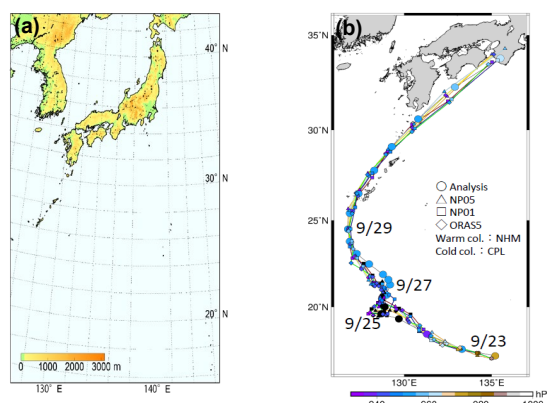Figure 1. (a) Computational domain. (b) Results of track simulations along with the RSMC Tokyo best track positions.
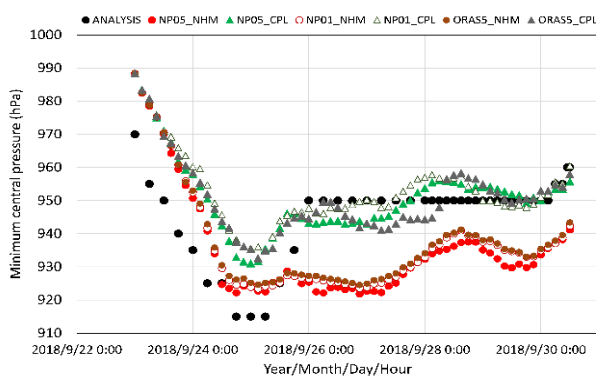

Figure 2. Time series of simulated central pressures (hPa) along with the RSMC best track central pressures.

Figure 2 shows the timeseries of simulated central pressure along with the RSMC best track central pressure. The increase in simulated central pressures due to ocean coupling was clearly found in all the experiments with the three oceanic reanalysis data sets (FORA, JPN, and ORA5). The difference in simulated central pressures between NHM and CPL became constant after the rapidly weakening of simulated Trami. At that time, the simulated central pressure became low again probably due to poor simulation of the mesoscale cold eddy around (21˚N, 129˚E). After 27 September, the simulated central pressure increased again in all the experiments, which was not found in the RSMC best track analysis.
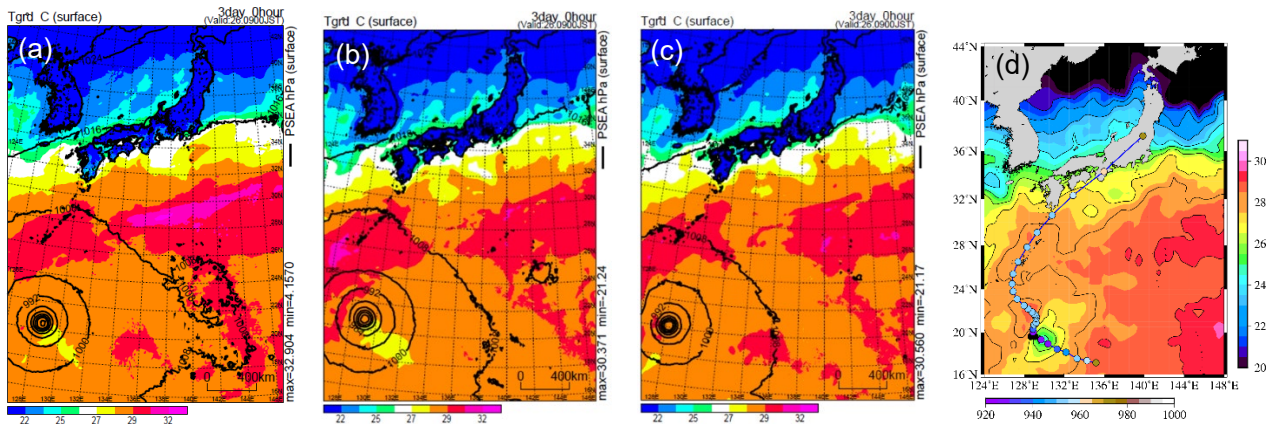

Figure 3. Horizontal distribution of simulated sea surface temperature and ground temperature in (a) NP05_CPL, (b) NP01_CPL, and (c) ORA5 experiments and (d) that of daily sea surface temperature (v05.0) obtained from the Remote Sensing Systems website (https://www.remss.com/measurements/sea-surface-temperature/).

Figures 3a-c show the horizontal distributions of simulated sea surface temperature and ground temperature in the NP05_CPL (Fig. 3a), NP01_CPL (Fig. 3b), and ORA5_CPL (Fig.3c) experiments. Compared with the horizontal distribution of daily sea surface temperature shown in Fig. 3d, Trami-induced sea surface cooling formed before the arrival of the stagnant area of Trami was poorly simulated in all the experiments. This may be caused by insufficient simulated peak intensity of Trami as well as uncertainty of the upper oceanic condition.

As for the insufficient peak simulated intensity, the central pressure at the initial time was relatively high in all the simulations compared with the RSMC best track central pressure (Fig. 2). This resulted in relatively high simulated central pressure during the intensification phase compared with the best track central pressure although the intensification rate was reasonably simulated particularly in the CPL simulations. This also means that the peak intensity in all the simulations calculated by the CPL was weaker than the best track analysis due to the relatively weak intensity at the initial time. Therefore, the ocean response to simulated wind stress of Trami continued to be relatively weak so that Trami-induced simulated sea surface cooling was not remarkable in the simulations shown in Figs. 3a-c. Nevertheless, this does not explain why Trami-induced sea surface cooling was least noticeable in the ORAS5_CPL experiment. On 27 September, simulated central pressure in the ORAS5_CPL experiment was lower than that in the other two experiments (NP01_CPL and NP05_CPL).

4. Concluding remarks

Sensitivity numerical experiments on the oceanic initial condition were conducted by the NHM and CPL with three different ocean reanalysis products. The use of the coupled model is important in predicting the intensity of Trami. In addition, the importance is independent of a kind of oceanic reanalysis datasets that is needed to create oceanic initial condition. However, any oceanic initial condition did not realize the improvement of the simulation of Trami's peak intensity. This may be in part due to unrealistic initial central pressure. Therefore, another numerical experiments using a different atmospheric analysis data different from the objective analysis in the Japan Meteorological Agency are needed. This will be a subject in the future.

References

Hirose, N., N. Usui, K. Sakamoto, H. Tsujino, G. Yamanaka, H. Nakano, S. Urakawa, T. Toyoda, Y. Fujii, and N. Kohno (2019) Development of a new operational system for monitoring and forecasting coastal and open ocean states around Japan. Ocean Dynamics, 69, 1333-1357.

Lea, D. J., I. Mirouze, M. J. Martin, R. R. King, A. Hines, D. Walters, and M. Thurlow (2015) Assessing a new data assimilation system based on the Met Office coupled atmosphere-land-ocean-sea ice model. Monthly Weather Review, 143, 4678–4694.

Usui, N., T. Wakamatsu, Y. Tanaka, N. Hirose, T. Toyoda, S. Nishikawa, Y. Fujii, Y. Takatsuki, H. Igarashi, H. Nishikawa, Y. Ishikawa, T. Kuragano, and M. Kamachi (2017) Four–dimensional variational ocean reanalysis: A 30–year high–resolution dataset in the western North Pacific (FORA–WNP30). J. Oceanogr., 73, 205–233.Wada, A., N. Kohno and Y. Kawai (2010). Impact of wave-ocean interaction on Typhoon Hai-Tang in 2005. SOLA, 6A, 13-16.

Wada, A. (2019) The impacts of preexisting oceanic cold eddies on the intensity forecast of Typhoon Trami (2018) during the mature phase. Research Activities in Atmospheric and Oceanic Modelling, 49, 9-11.

Wada, A. (2021) Roles of oceanic mesoscale eddy in rapid weakening of Typhoons Trami and Kong-Rey in 2018 simulated with a 2-km-mesh atmosphere-wave-ocean coupled model. Journal of the Meteorological Society of Japan, 99, 1453–1482.